CHALMERS

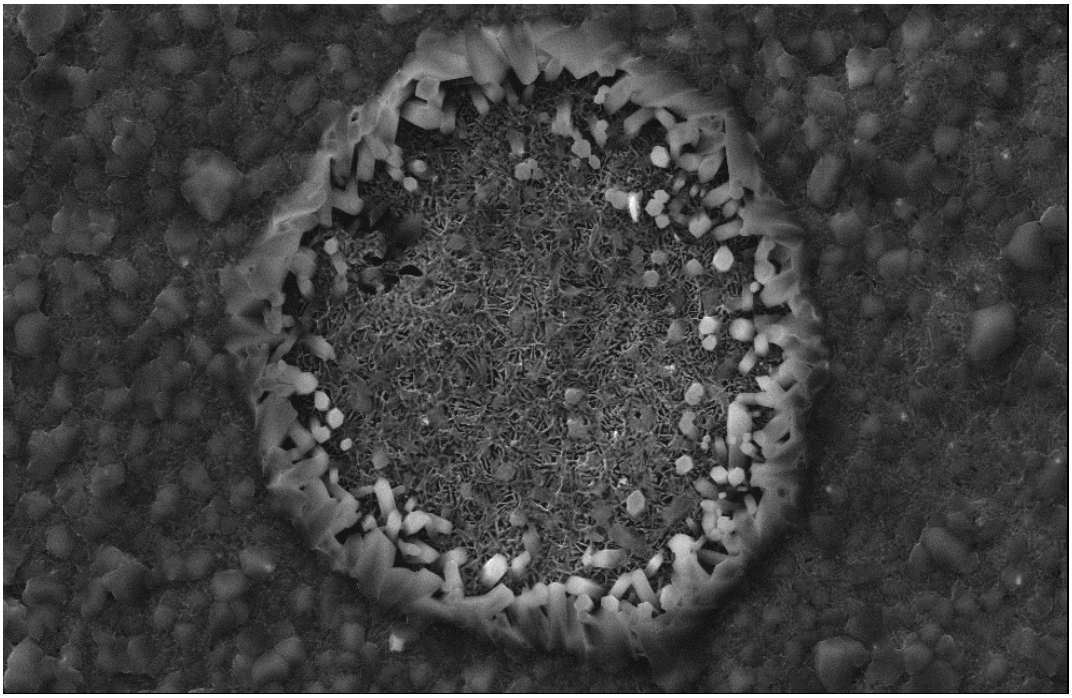

The effect of K_2CO_3 on the high temperature corrosion of a FeCrAl alloy

Bachelor of Science Thesis

JOHNNY VIITALA

The High Temperature Corrosion center

Department of Chemical and Biological Engineering

CHALMERS UNIVERSITY OF TECHNOLOGY

Gothenburg, Sweden, 2013

The effect of K_2CO_3 on the high temperature corrosion of a FeCrAl alloy

JOHNNY VIITALA

The High Temperature Corrosion Centre, HTC

Department of Chemical and Biological Engineering,

Chalmers University of Technology

Gothenburg, Sweden

Cover:

A part of the corroded metal surface showing Fe_2O_3 in the center and K_2CrO_4 grains in the surrounding area (p.15).

Gothenburg, Sweden, 2013

The effects of K_2CO_3 on the high temperature corrosion of a FeCrAl alloy

JOHNNY VIITALA

Department of Chemical and Biological Engineering

Chalmers University of Technology

Gothenburg, Sweden

Summary

The world of today is in a great need of energy, and new sources of energy are required. Two of these are waste and biomass being incinerated in waste and biomass fired boilers. KCl forms in both of these and corrodes the inside of the plant facility. Currently it is unknown if the potassium or the chloride is the most corrosive. If the effects of K_2CO_3 can be found out, the relative corrosiveness of K^+ can be determined since no Cl^- is present. The goal of this project is to determine the effects of K_2CO_3 on the high temperature corrosion of a FeCrAl alloy.

The effects of K_2CO_3 on the high temperature corrosion of a FeCrAl alloy were investigated at 600°C for 1-168 hours. The exposures were performed in a horizontal tube furnace and the kinetics was tracked by weighing the samples before and after exposure. The formed oxide products were examined using x-ray diffraction, ion chromatography and scanning electron microscopy with energy dispersive x-ray spectroscopy.

The visual inspection rendered no useful results as no visible systematic corrosion could be discerned. The mass gain increased sharply in the beginning but then at 24h the mass gain was linear at a slower rate. The XRD show that the amount of K_2CrO_4 increase continually until a peak is reached at 72h. Thereafter the amount of K_2CrO_4 is diminished. The Fe_2O_3 have no systematic increase or decrease but is always present at the surface except for on the unexposed sample. The IC have a similar peak of K_2CrO_4 but is present at 24h instead. The SEM showed K_2CO_3 formations on the unexposed salted samples. Traces of these remain on the sample exposed for 1 h and the smooth surface of the unexposed sample has been replaced by an almost completely covering layer of K_2CrO_4 grains (the base oxide). Small craters in the base oxide can be seen after exposure up to 24h. After longer exposure times no unreacted K_2CO_3 is left, in their stead there are white dotted areas rich in Si. Small areas of pointy Fe_2O_3 can be seen on the samples exposed for 72h. These areas can be seen to be larger on the samples exposed for 168h.

The result was that the metal forms a non-protective K_2CrO_4 oxide layer that starts to disappear between 24 and 72 hours. The mechanism of K_2CrO_4 formation is described, but the disappearance is still unknown. Of particular interest was that Si oxide formed on the surface, a theory being that an increased amount of Si could form a protective oxide layer.

Table of Contents

1. Background

The world society of today is extremely dependent on non-renewable energy. From the cars that drive on gasoline to coal and nuclear power that generates power, none of these power sources are truly bottomless. Two common alternative energy sources are waste and biomass combustion.

In traditional energy plants many components are manufactured of FeCr-steels. The FeCr-alloy forms an oxide layer (chromia) that protects the metal from further corrosion in these environments. However, biomass and waste contains K and Cl that reacts with the chromia and prevent it from forming a protective scale. In attempt to find a material with a longer lifetime, an alumina forming material (FeCrAl alloy) has been studied in these types of environments. The FeCrAl alloys has been shown to be superior to FeCr alloys in these environments. However, the corrosion is far from completely inhibited by the alumina scale. It is however not known which species is the more corrosive one, the potassium or the chloride. By studying the high temperature corrosive effects of K_2CO_3 on the steel the effects of potassium can be determined.

Kanthal® APMT is a FeCrAl steel that forms an aluminum protective layer at higher temperatures. FeCrAl is normally used in ranges from 900-1300˚C where the previously mentioned alumina protective layer forms. At lower temperatures a metastable alumina is formed with less protective properties.

The goal of this project is to examine the effect of K_2CO_3 on the high temperature corrosion of Kanthal® APMT.

2. Theory

Corrosion is a result of interaction between the metal and the surrounding environment. In the natural environment metals are almost never present in pure form. Instead metal exist in the form of oxides (commonly known as ores). If a piece of metal is left alone it will slowly return to its native form. Rust and ore are very similar in chemical composition.[i]

2.1 Thermodynamics

In Formula 1, the corrosion reaction between metal, M, and oxygen gas, O_2, is written.

$$xM(s) + \frac{y}{2}O_2(g) \rightarrow M_xO_y(s) \qquad (1$$

The arrow in the reaction does not signify that the reaction necessarily happens, as there are outside factors deciding if corrosion occurs.[ii] The direction can be determined from the second law of thermodynamics, found below in Equation 1.

$$G' = H' - TS' \qquad (1$$

G' is the Gibbs free energy of the system, H' is enthalpy, T is temperature and lastly S' is the entropy during constant temperature and pressure. Negative values on G' means a spontaneous reaction takes

place whilst positive G' indicates that no reaction occurs. Reaction 1 and equation 1 can be combined and will yield the following formula 2:

$$\Delta G' = \Delta^{\circ} G + RT ln \left(\frac{a M_x O_y}{a_{Mx} \, a O_2^{\frac{Y}{2}}} \right) \quad (2$$

Equation 2 contains Δ˚G which is standard free energy change; R is the ideal gas constant and T is the temperature in Kelvin. Equation 3 on the other hand can calculate the standard Gibbs free energy, Δ°G, using the energies of formation for the involved element types.

$$\Delta^{\circ} G = G^{\bullet} a M_x O_y - x G^{\circ}{}_M \frac{Y}{2} G^{\circ}{}_{O_2} \quad (3$$

2.3 Kinetics of oxidation

As metal oxidizes, it will gain weight as it binds oxygen to the surface. There are three different kinds of ideal mass growth rates that are possible; linear, parabolic or logarithmic and can all be seen in Figure 2. The growth rate is decided by temperature, oxygen pressure, elapsed time of reaction, surface preparation, and pretreatment of the metal. Knowledge of the kinetics alone is not enough to know which exact reaction that occurs, but it is a good supplement and can help narrow down the amount of possible reactions. Each type will be examined from the bottom to the top as listed in Figure 1.

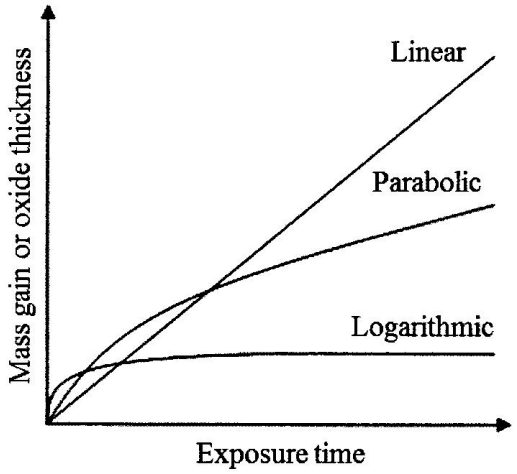

Figure 1: Logarithmic, parabolic and linear rate equation

2.3.1 Logarithmic rate equations

The logarithmic rate equation is common for metals exposed to low temperatures (300°C-400°C). It is initially rapid and then slows down to low or negligible levels. The actual equation can be seen below as equation 4 and 5.

$$\textbf{Direct logarithmic: } \mathbf{x} = k_{\log} \square_{\log}(t + t_0) + A \quad (4$$

Inverse logarithmic: $\frac{1}{x} = -(k]_{il} \log[(t)) + B$ (5

The x in the above equations can stand for several things: the thickness of the oxide film, the amount of oxygen consumed per unit surface area of the metal or the amount of metal transformed to oxide. The t is the time variable whilst k_{log} and k_{il} is rate constants. Lastly A and B are constant. Several theories have been suggested to explain the rate determining step such as transport of electrons, chemisorption, or cavity formation in the film.

2.3.2 Parabolic rate equation

In contrast to the lower temperature previously mentioned, parabolic rate equations is more common at higher temperatures. The main difference between the logarithmic and parabolic equation is that whilst logarithmic almost stops entirely, the parabolic rate continues and relies on another rate determining mechanism. Equations 6 and 7 below show both the differential and the integral version.

$$\frac{dx}{dt} = \frac{k'_p}{x} \quad (6$$

$$x^2 = 2k'_p t + C = k_p + C \quad (7$$

The k'_p and k_p is parabolic rate constants whilst C is the integration constant. If the metal has a parabolic growth rate, this usually denotes that the rate determining mechanism is the diffusion of reactants trough a growing oxide layer, either oxide ions inwards or metal ions outwards. This is however explained in greater detail in "2.4 Mechanism of corrosion".

2.3.3 Linear rate equation

Last of the three ideal equations, is the linear rate equation. The differential and integral form of the linear rate equation is shown below, equation 8 and 9

$$\frac{dx}{dt} = k_1 \quad (8$$

$$x = k_1 t + C \quad (9$$

The linear rate equation does not change growth rate with time, since it is not at all restricted by the growing oxide thickness. Instead it usually depends on the adsorption of oxygen to the surface; a reaction governed by the steady state formation of oxide at the metal/oxide interphase or simply has an oxide that is at a constant thickness.[ii]

2.4 Mechanism of corrosion

The mechanism of corrosion initiates with oxygen molecules adsorbing onto the oxide free metal surface, forming single disassociated atoms (Figure 2, step 1). In the second step one can see the beginning stage of an oxide layer. The absorbed oxygen attracts electrons and become chemisorbed. Subsequently the oxygen turns into oxide that forms in a few areas and spread laterally until a continuous oxide film forms. For the corrosion to continue, the reacting species must diffuse through the oxide layer.

The oxide can either grow at the upper oxide surface to the air, or in the lower oxide surface, against the metal. This is respectively called outwards growing oxide and inward growing oxide. The outward growing oxide depends on the metal ions to travel out to the outer surface to react with the oxygen whilst the inward growing oxide depends on the oxygen ions to diffuse through the oxide and react with the metal. Both reactions require electrons to travel through the oxide. All these different growth types can create different tensions in the oxide.[i]

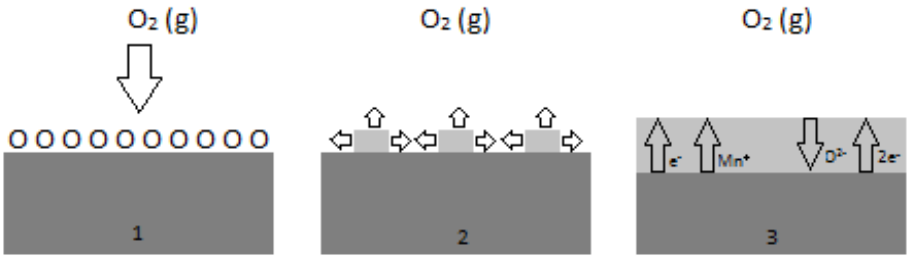

Figure 2: Oxide formation

2.2 Defect diffusion

Oxides consist of metal ions and oxide ions formed in a lattice. The lattice is not perfect and has several breaks in regularity. These defects in conjunction with micro cracks and grain boundaries are the only way for the ions to transport trough the oxide layer.

Lattice defects are the major contributor to ion migration at higher temperature (above 100°C). Also known as point defects these can be seen in Figure 3. There are two main kinds of point defects, vacancy (A) and interstitial (B) defects. Depending on the atoms relative size and what structure the oxide has, the diffusion vary.[ii]

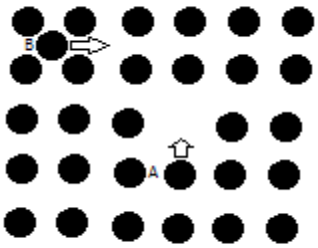

Figure 3: Schematic of defect diffusion

2.5 Oxidation of pure metals and alloys

2.5.1 Single metals

To understand the corrosion of alloys, it is an advantage to first know the corrosion of the single metals of the steel. For a FeCrAl alloy, studied in this work, that is iron, chromium and aluminum.

At temperatures below 570°C, iron forms a dual layer of Fe_2O_3 and Fe_3O_4. At temperatures above 570°C iron form a triple layer with the previous two oxides and an additional layer of FeO.

When chrome oxidizes it forms Cr_2O_3. This is a very protective oxide, but there are some complications. At temperatures above 850-900°C the gaseous specie CrO_3 form. In addition, in the presence of water vapor the gaseous specie $CrO_2(OH)_2$ forms. The formation of these gaseous species prevents a protective Cr_2O_3 scale to be established on the material surface. This limits the effective use of chrome steel to temperatures below 900°.

Aluminum always forms a thin oxide layer at room temperature with a thickness of 2-3 nm. At temperatures less than 350°C an amorphous film forms that has an inverse logarithmic kinetic. Between 350°C to 425°C the film changes kinetics to parabolic.[ii] Above 425°C the corrosion mechanism becomes a lot more complex as aluminum has several different oxide forms. θ-Al_2O_3, γ-Al_2O_3, δ-Al_2O_3, are all meta stable, whilst α-Al_2O_3 is stable. α-Al_2O_3 also has fewer defects which results in a more protective scale. At higher temperatures, around 1000°C, α-Al_2O_3 usually form and metastable Al_2O_3 transforms into α-Al_2O_3. The meta stable Al_2O_3 are common at lower temperatures and may form initially at higher temperatures. [iii]

2.5.2 Corrosion of alloys

Alloys, a mixture of several different metals and possibly other materials as well, have a more complex corrosion behavior than single metals. The initial stage is very similar, but from then on these are some factors affecting the corrosion:

1. Amount of either metal
2. Either metals affinity for oxygen
3. Difference in metal diffusivity in the alloy

First a thin oxide mixture of all metals will be present on the surface. The least noble metal, the one with the highest growth rate, usually outgrows the other and forms an oxide layer alone. This corrosion reaction can also reduce the other oxides to metal and thus completely replace the more noble metal oxide. If the concentration of either metal is low, the corrosion favors the other metal oxides. However, if composition and oxide growth is the same, both oxides may form which results in a mixed oxide.[ii]

3. Material and equipment

This work has the requirements of materials, several tools and instruments to analyze the corrosive effects of K_2CO_3. Here follows an overview of all equipment used during the project.

3.1 The FeCrAl alloy

The material investigated in this work is Kanthal® APMT (Advanced Powder Metallurgy Technology) supplied by Sandvik heating technology and is from now on referred to as APMT. This alloy is a mixture of many different elements as seen in Table 1. APMT has good mechanical properties compared to conventially cast FeCrAl alloys since APMT is dispersion strengthened and thereby grain size controlled. The metal grain growth is inhibited by small (20-200 nm) inclusions of oxides, carbides and nitrides that

prohibit grain growth to a size of about 10-20 µm. The alloy is produced using a technique called RSP, rapidly solidifying powder.[v]

Table 1: Steel Composition[v]

Composition APMT	Cr	Al	C	Mn	Si	Minor additives	Fe
wt.%	21.0	5.0	0.08	0.4	0.7	Y, Zr, Hf	bal.
at.%	21.2	9.7	0.4	0.4	1.3		bal.

3.2 Horizontal tube furnace

The furnace used in this work is a horizontal tube furnace.

The gas flow to the furnace is at 1000 ml/min and the composition of the gas is 5% O_2, 40% H_2O and 55% N_2. These gases, except for the water, originate from large tanks kept separate from the furnace. As can be seen in Figure 4, the gas flow is mixed at point A and then go to B, the humidifier with a set temperature of 79,3±0,2˚C. The gas is then forced up through the heat exchanger, C, out in the plastic tubing and to the glass tube that is set in the furnace, D. The heat exchanger is fed with water at a temperature of 76,3˚C removing excess water from the gas flow. This container is located at point E. Both the humidifier and the heat exchanger need to be filled with water with regular intervals. All plastic tubing after the heat exchanger and the glass furnace parts outside the furnace is kept warm with heating cords at 80 ˚C to avoid water condensation. They are also covered in aluminum foil to keep the heat evenly distributed across the tubing surface.

A SiO_2 glass tube is set in the furnace, F. The tube has a diameter of 5 cm and a length of 120 cm with a removable glass cover at G. The maximum temperature is measured to 600.4˚C ±0.5˚C in point H, positioned 52,2 cm from the tube opening. This point is also where the sample always was positioned during the exposure.

After the gas exits the tube it is led through more heated plastic tubing to a container, I, that bubbles the gas through room temperature water. This creates a slight overpressure that prevents any gas in the environment to leak into the system. The previously mentioned water container needs frequent emptying. Then the gas is let out to the surrounding atmosphere at point J.

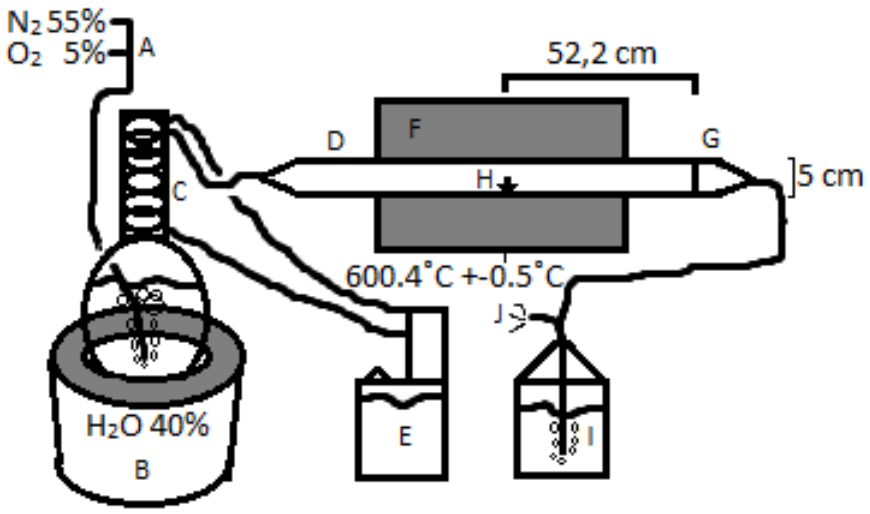

Figure 1: Schematic of a tube furnace

3.3 X-Ray Diffraction

The X-Ray Diffraction (XRD) is the most commonly used method for determining the oxide layer's crystalline structure and was used in this work to determine the crystalline oxide products formed.

The molecular structure of the metal is a three dimensional crystal structure. Because of the ordered formation it can be described as consisting of many planes of atoms. This is illustrated in Figure 5 with two rays of light that first enter and then reflect off two different atomic planes. Ray number one reflects off the first layer whilst the second ray reflects on the lower second plane. This creates a difference in path length of "a". If "a" is not equal to the wavelength, destructive interference occurs and thus the x-rays that exit the crystal will be weaker. If "a" is equal to the wavelength they're in phase and therefore positively reinforced. The instrument detects these peaks in amplitude.

The detector is constructed to scan which means that the rays from several different angles are detected. Thus the wavelength and angle will be known and with the help of Braggs law the distance between atomic planes can be calculated.

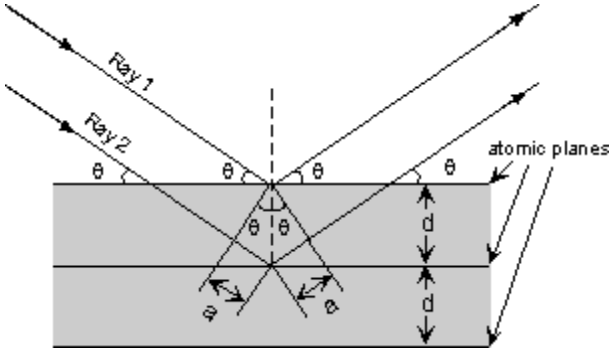

Figure 2: Schematic of XRD x-ray reflection

The detected diffraction patterns is compared to and thus determined with a database called Powder Diffraction File.[vi]

In this work, the corrosion product formed on the metal after exposure was analyzed with Grazing-Incidence X-ray Diffraction (GI-XRD) using a Siemens D5000.

3.4 Scanning Electron Microscopy

Scanning Election Microscopy (SEM) is a tool for analysis used to acquire information about the surface structure and composition. SEM functions in a similar way as common microscopes, but instead of using electromagnetic radiation in the visible spectrum, SEM uses an electron beam that increase the maximum amount of magnification by several magnitudes.

The previously mentioned ion beam is produced in an ion source (filament) that is charged with a high amount of current. The ion beam is aimed down a column with several electromagnetic lenses, and hits the sample. Secondary electrons gives contrast due to the topography (edges are brighter than flat regions) whilst backscattered electrons gives contrast due to the elemental composition; a brighter area contains heavier elements.[vii]

3.5 Energy Dispersive X-Ray Spectroscopy

Energy dispersive x-ray spectroscopy (EDX) is an analytical technique to determine the elemental composition of a sample and is commonly used in conjunction with SEM. The sample is lit up with a particle beam and the resulting X-ray spectrum depends on the atomic structure of the atoms that are hit. This is thus a very precise technique.[iii]

In this work the samples were examined using a FEI Quanta 200 FEG ESEM quipped with oxford INCA EDX system. For imaging and EDX analysis an accelerating voltage of 10 – 20 kV was used. This instrument was used both for the SEM and EDX.

3.6 Ion Chromatography

Ion Chromatography (IC) is a method to determinate the concentration of several different ions in a solution. The sample solution is run through an analytical column composed of a tube with ions bound to the inner area. Depending on the charge of the ion analytes they will bind to the ions of the tubing more or less. This together with the size of the ions will separate them which allows for a detection of the different species with a conductivity detector. The analyzed ions can then be determined with the help of running standard solution trough the column and comparing results.[ii]

The ion chromatograph used was a Dionex ICS-90 and it was used to determine the amount of K_2CrO_4 present in the sample. The column was a 4mm IonPacAS4A-SC. A solution of $1.8mMNa_2CO_3/1.7mMNaHCO_3$ was used as eluent. The flow rate was 2ml/min whilst the detection limit of CrO_4^{2-} was at 0.01 µmol. The sample solution was prepared by leaching a metal sample in 10ml of water in an ultrasonic bath for 10 minutes. After the sample water was filtrated, it was diluted five times and subsequently analyzed in the column.[viii]

4. Method

4.1 Sample preparation

It is of great importance that all samples have the same surface finish to eliminate variances in oxidation rate. Therefore all the samples where polished, cleaned and dried in the same way.

4.1.1 Sample Polishing

A 320 grit grinding paper was used to initially even out the rough edges, created during sample production. A Struers Rotopol-31 was used for this initial edge polishing, whilst subsequent polishing was done with a Struers TegraPol-31.

A dual layer of double-sided tape was used to stick the sample to the sample holder. The tape that stuck hard to the surface were placed on the holder, the tape that stuck hard to the sample where placed on top of that tape, and lastly the sample was place on top of the later tape. Ten samples was polished each run. After every step the samples were cleaned, whilst attached to the sample holder, using detergent, water and lastly rinsed with distilled water and then dried. The first step used the same grinding paper as the step above, 320 grit. This step was run for 40s and then the samples were examined. If any clearly distinguishable scratches were present, all samples were grind for another 40s. The remaining polishing was done with DP Blue and diamond solution in three steps for four minutes each. The polishing discs were used in the order of Largo 9µm, Dac 3µm and lastly Nap 1µm. When both sides of the sample where polished the washing process was initiated.

4.1.2 Washing

For the washing procedure, the samples were put into a beaker with several holes for holding samples. These where then filled with distilled water and the whole beaker was subsequently put into an ultrasonic bath for 10 minutes. The cleaning procedure was repeated with acetone and finally ethanol. The samples were then dried with flowing air and stored in small plastic bags.

4.1.3 Weighing and Salting

Before exposure, the samples were weighted and salted. The amount salt (K2CO3) that was applied on a sample was 6116µg. This amount salt was chosen since it corresponds to the amount KCl applied to a similar FeCrAl sample in another investigation. This makes it easy to compare the results and the effect of K versus Cl.

The mass was measured using a balance. The weight of each sample was recorded five times and the average was calculated. This technique was used for the clean samples and for the exposed samples.

The salt solution was a simple mixture of distilled water and K_2CO_3 salt, initially concentrated until saturation. This was however not possible as K_2CO_3 is extremely soluble, so the solution was mixed with water until found suitable. The sample was weighed without salt and then weighed with salt applied by spraying a K_2CO_3 solution. The aim was an even application of salt over the metal surface.

The samples were one by one sprayed with salt, dried and weighed. This procedure was repeated until found to be within ~20µg of the required mass. If the salt mass was found to be too high, the sample was discarded for cleaning and reuse. The salted samples were kept in the desiccator until exposure.

There where however a factor complicating the matter, K_2CO_3 is very hygroscopic and water vapor in the air quickly adheres to the salt. This makes weighing a challenge as the salt continually absorbs more water. The water mass increase requires the weighing to be as fast as possible, whilst the sample need time to stabilize as previously mentioned. The salt weight was read immediately the first time the scale was somewhat stable.

4.2 Exposure

The samples were exposed in the furnace either immediately after salting or at most the day after depending on time available. The samples are put in the middle of the slits on sample holder, seen as point 1-3 according to Figure 6. The sample holder itself is positioned on the boat underneath that can be seen as a pencil formed shape. The boat is then placed in the furnace so that the middle point was 52,2 cm from the opening. The samples are exposed for 1, 24, 72 and 168 hours. Each exposure was repeated once with new samples to increase accuracy. They are weighted again post-exposure.

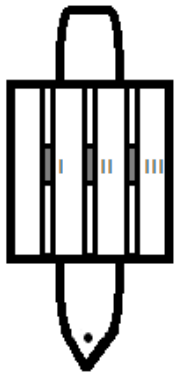

Figure 3: Simple schematic of an sample holder positioned on boat

5. Results

5.1 Visual inspection

Pictured in Figure 7 is an example of the surface of the sample as it changes with increased exposure time. The surface change is highly irregular and no clearly visible system of corrosion can be easily discerned.

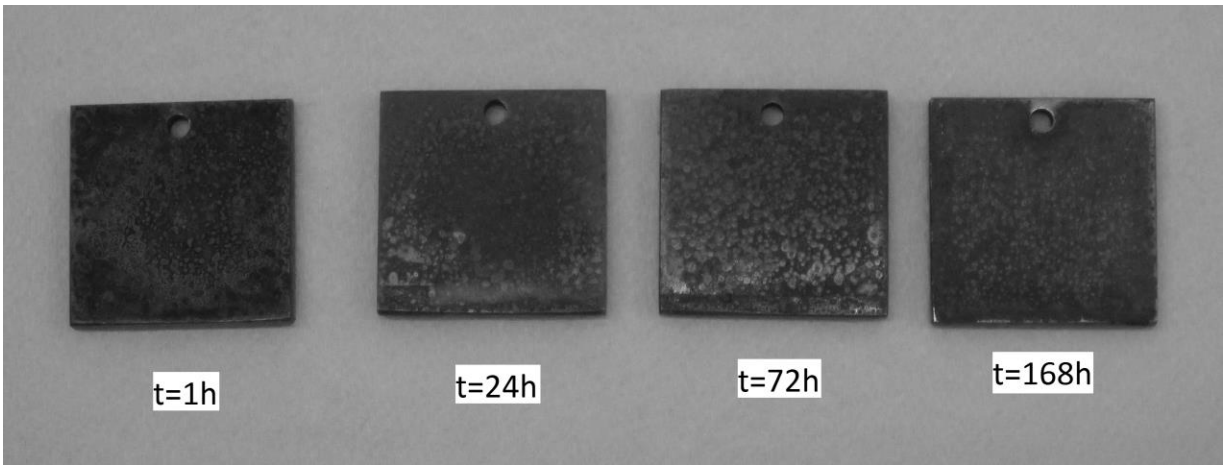

Figure 4: Examples of surface structure from APMT material applied with K_2CO_3 exposed for 0-168h at 600°C in O_2+H_2O.

5.2 Mass gain

In Figure 8 the average mass gain over time is depicted. The mass gain is fast initially and declines with exposure time. After 24 hours of exposure the mass gain appears linear. The variance can be seen in as the staples that are found crossing the average mass gain point and is at average around 25µg/cm^2.

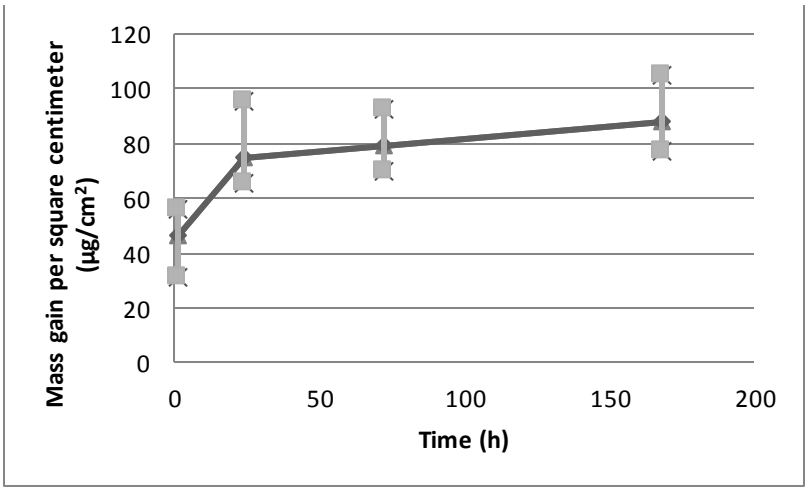

Figure 5: Mass gain graph of APMT material applied with K_2CO_3 exposed for 0-168h at 600°C in O_2+H_2O.

5.3 X-Ray Diffraction

Figure 9 shows peaks corresponding to Fe_2O_3 and K_2CrO_4 during different times. The sample exposure times where; unexposed, 1 hour, 24 hours, 72 hours and lastly 168 hours. Two peaks are seen on all the samples and are attributed to the base material. The unexposed salted sample only shows peaks corresponding to the base material. The applied K_2CO_3 on the other hand is of many different forms resulting in a great difficulty to find peaks that correspond with it.

In Figure 9 the grey lines can be seen as iron oxide. The amount doesn't seem to increase in a specific way, but is always present except for on the unexposed sample. The black lines at the bottom of Figure 9 represent the peak intensity and position for K_2CrO_4. A clear trend can be seen for the peaks

corresponding to K_2CrO_4 on the exposed samples. The amount of K_2CrO_4 steadily increases up to the 72h sample. However, at 168h we can see a large decrease of K_2CrO_4.

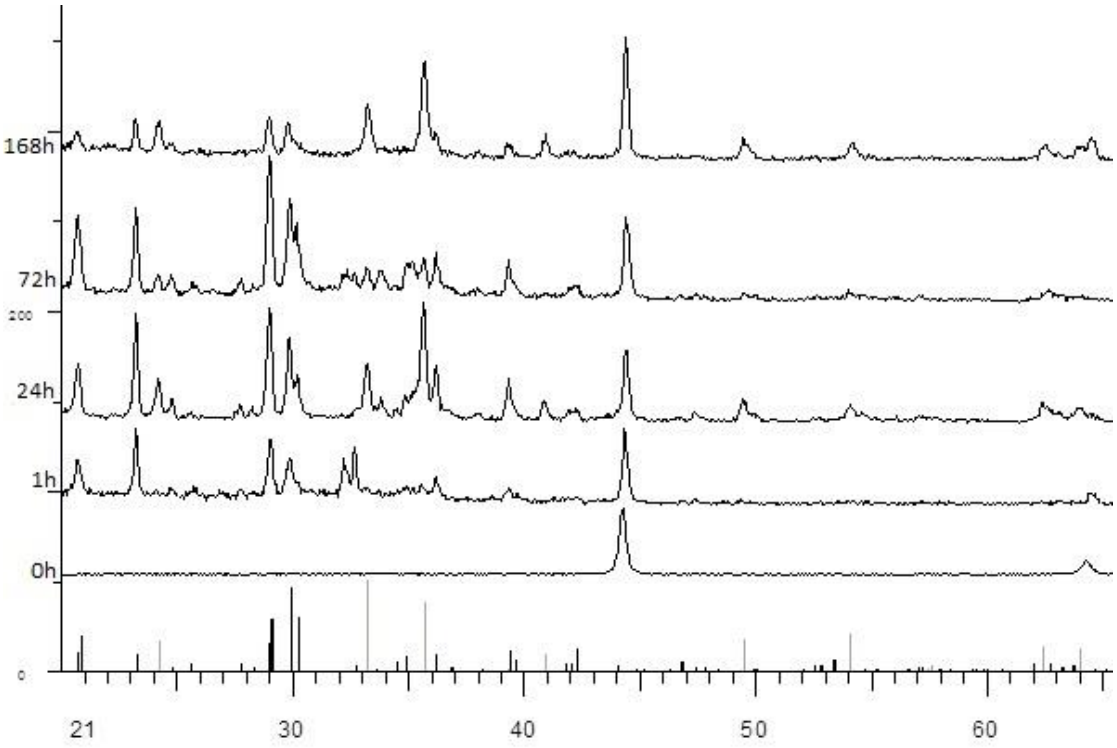

Figure 9: X-ray diffraction pattern of APMT material applied with K_2CO_3 exposed for 0-168h at 600°C in O_2+H_2O.

5.4 Ion Chromatography

Figure 10 illustrates the results of the IC analysis. Data for both area (higher line) and height (lower line) of the chromatogram peaks show similar results. The measured K_2CrO_4 mass can be concluded to be at its highest around the exposure time of 24 hours and decrease considerably thereafter. This is not consistent with the XRD, which will be discussed in the conclusion.

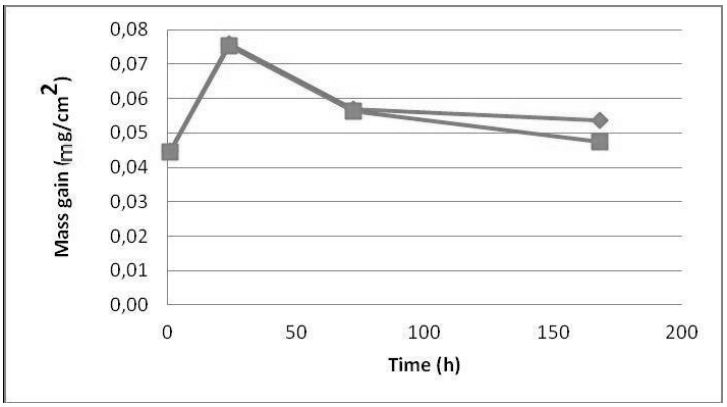

Figure 10: Ion chromatography of APMT material applied with K_2CO_3 exposed for 0-168h at 600°C in O_2+H_2O.

5.5 Scanning Electron Microscopy

Figure 11 shows an overview of all the samples in order from shortest exposure time to the longest. The magnification is 200 on all samples except figure 11.5 that have a magnification of 500. All images are taken in the secondary mode except the unexposed sample that is taken in the backscattered mode.

In Figure 11.1 the surface of an unexposed salted sample is shown. K_2CO_3 particles can be seen as black dots, marked A in the image. The size of the salt particles ranges from 1-100 µm. In Figure 11.2 the surface of a salted sample exposed for 1 hour is seen. Large black formations marked with A is shown by the EDX to be partly unreacted K_2CO_3. At subsequent exposure times, these areas form large areas of lighter oxide (Figure 11.2-5). At point B in figure 11, small circles of a lighter color can be seen. These are suspected to form into craters seen on the longer exposed samples (Figure 11.2-5), also marked with B. The areas marked A and B will be described further below. The base oxide, located between areas A and B, will also be described as the base oxide.

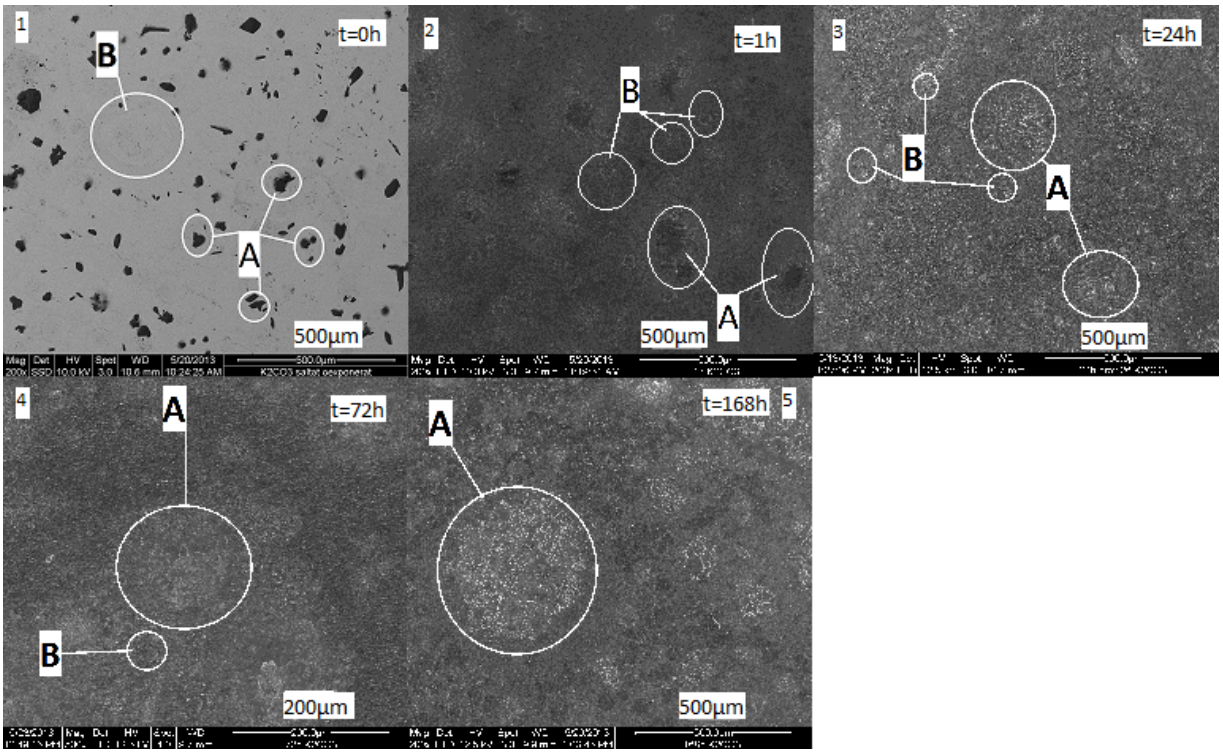

Figure 11: Scanning Electron Microscopy of APMT material applied with K_2CO_3 exposed for 0-168h at 600°C in O_2+H_2O.

5.5.1 Base oxide

All exposed samples form a continuous film of K_2CrO_4 and can be seen as the standard surface of the samples. The sample surfaces shown in Figures 12.1-2 are representative for the base oxides formed on samples exposed for 1h and 24h, respectively. Figure 12.4 show some darker areas on the 24h sample that show slight signs of iron oxide as can be seen on the SEM point analysis (p. 20) which are not present on the 1h sample. Figure 12.3 shows an area of base oxide with slightly darkened color from a sample exposed for 168h. The close-up in Figure 12.5 shows that the K_2CrO_4 grain is slowly hollowed

out, exposing iron oxide underneath. This in all indicates that the K_2CrO_4 grows but then deteriorates and in its place iron oxide forms.

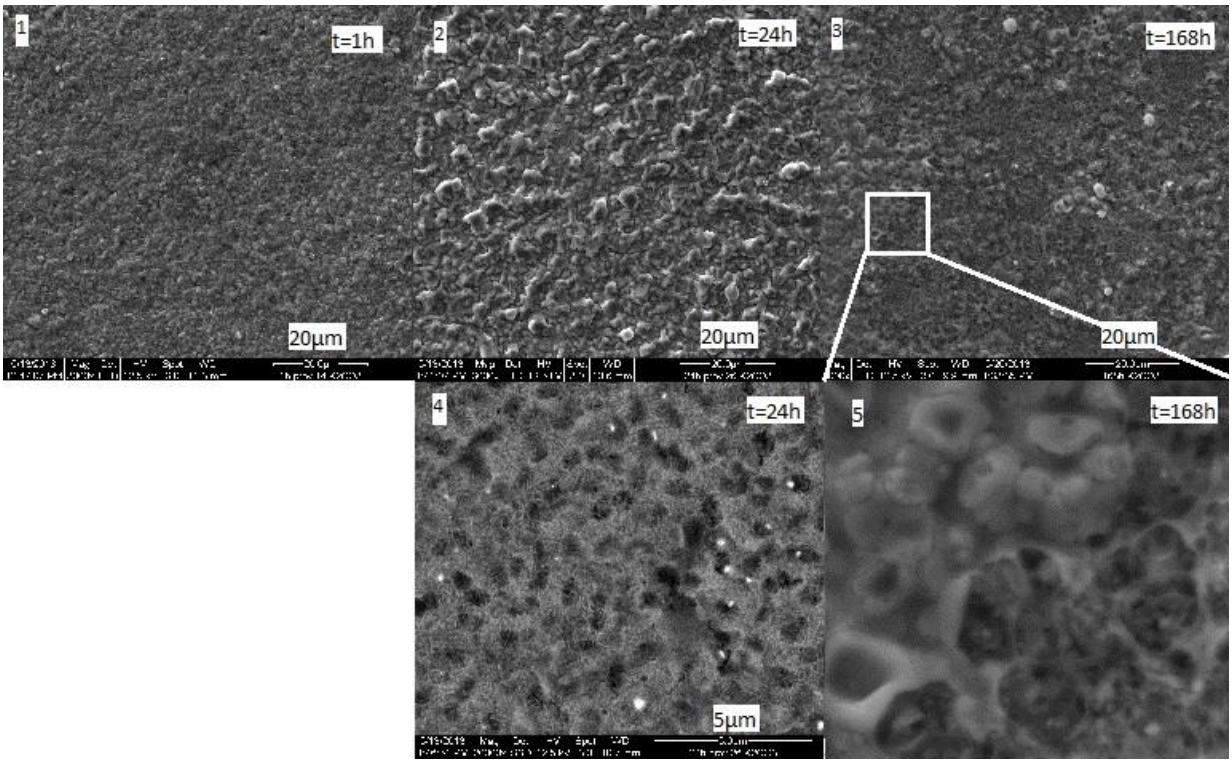

Figure 126: Scanning Electron Microscopy of APMT material applied with K_2CO_3 exposed for 0-168h at 600°C in O_2+H_2O

5.5.2 K_2CO_3 Formations

When the potassium carbonate solution is sprayed on the surface, the solution forms large drops that then evaporate and leave K_2CO_3 formations behind. These can be seen as dark areas on the surface of the sample exposed for 1h (see Figure 13.1). On the surface of the samples exposed for 24-168h, seen in Figure 13.2-3, the K_2CO_3 formations has disappeared and only large white areas remain, dominantly colored by silica rich white spheres that can be seen in a higher magnification in Figure 13.4.

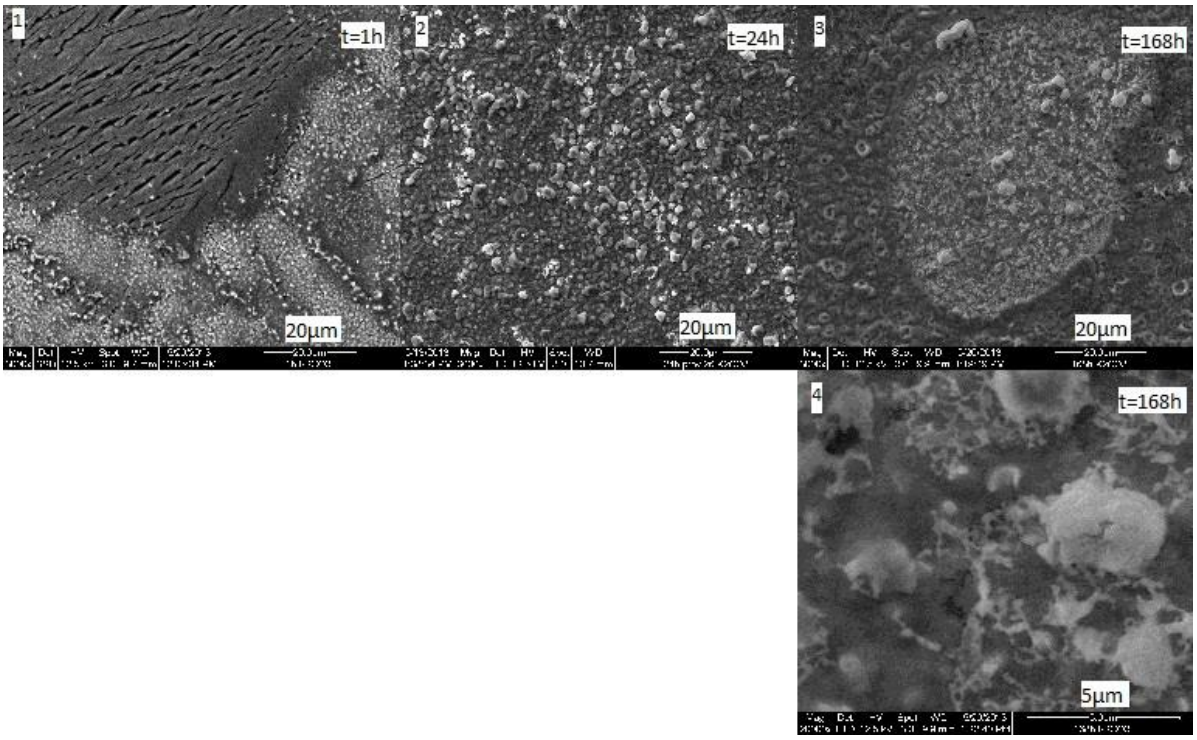

Figure 13: Scanning Electron Microscopy of APMT material applied with K_2CO_3 exposed for 0-168h at 600°C in O_2+H_2O.

5.5.3 Craters created by solution droplets

Circular hole-like formations is already visible on the surface of the sample exposed for 1h (Figure 14) but is much more pronounced after 24h exposure (Figure 15). These craters seemingly dissolve as there are no traces remaining on the sample exposed for 72h. On the unexposed samples, these "craters" are barely seen as darker rings. The craters on the 1h exposed sample and the edge of the craters on the 24h exposed sample seem to consist solely of K_2CrO_4. However, the inside of the craters on the samples exposed for 24h has a characteristically pointy structure and is identified as iron oxide, Fe_2O_3. This is also supported by the XRD that proves that there is iron oxide in this area.

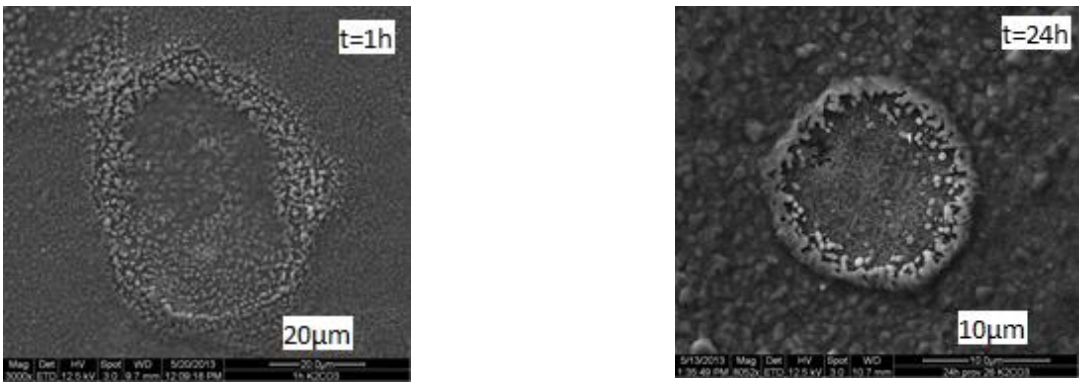

Figure 7 and 8: Scanning Electron Microscopy of APMT material applied with K_2CO_3 exposed for 1-24h at 600°C in O_2+H_2O.

5.6 Energy Dispersive X-ray Analysis

5.6.1 General Mapping

Figure 16 is the EDX mapping of the metal surface exposed for 24h. The surface seems to be largely homogenous in composition; a mixture of base metals, oxygen and small amounts of K. The only irregularities is the darker areas (marked as A in figure 16) encircled in the picture. The one element here seems to be K and C which as mentioned earlier, heavily implies this is partly unreacted K_2CO_3.

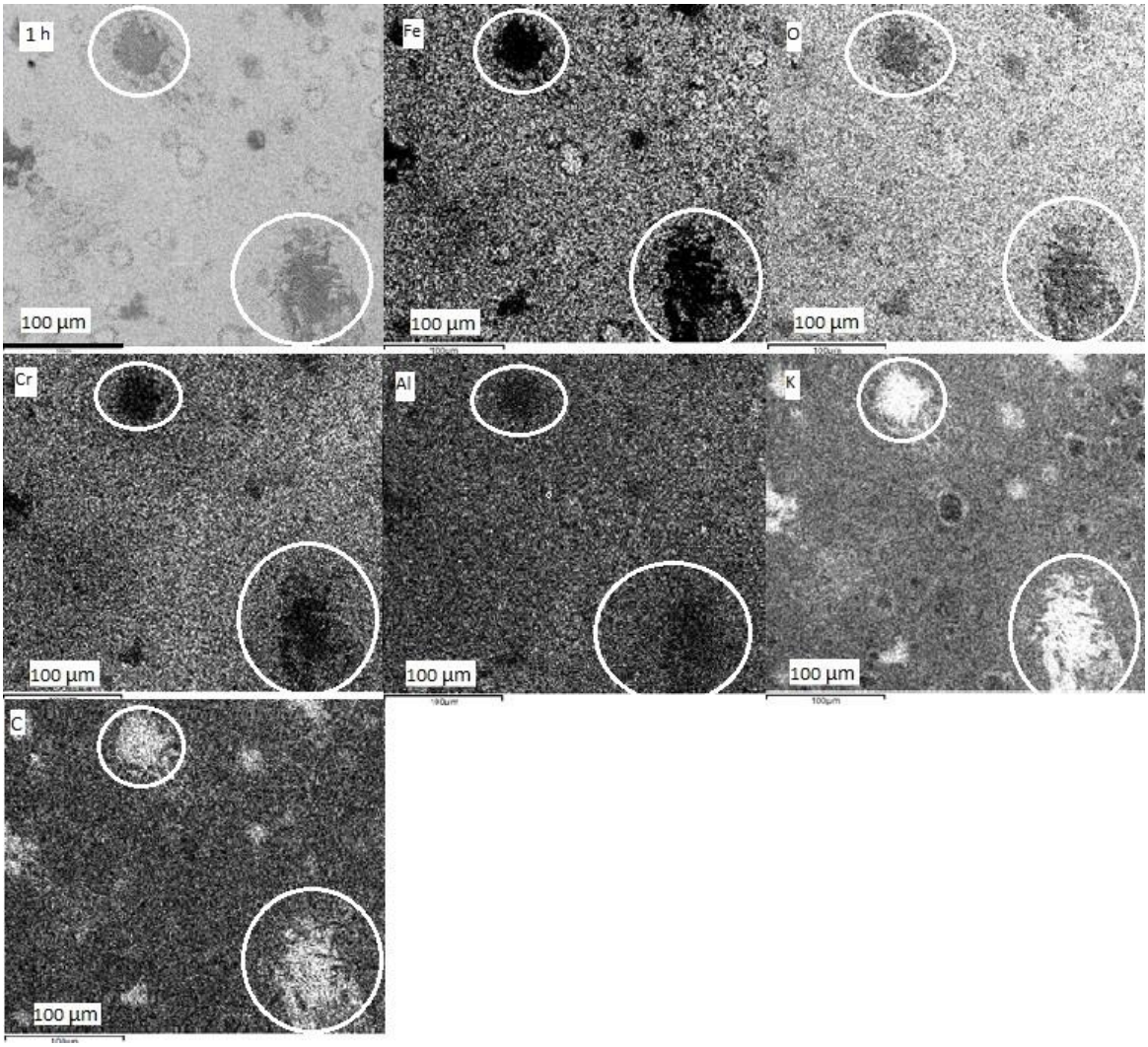

Figure 9: Energy Dispersive X-ray Analysis mapping of APMT material applied with K_2CO_3 exposed for 24h at 600°C in O_2+H_2O.

Figure 17 illustrates the chemical composition of the oxide formed on samples exposed for 168h. The surface is covered in K, and Cr. Large areas (A) appears to have a deficiency in K and Cr. Only oxygen, iron and small amounts of aluminum seem to be present, indicating the presence of iron oxide in these areas. This is confirmed by EDX point analysis. Small Si-rich blobs are present in small clusters across the entire surface.

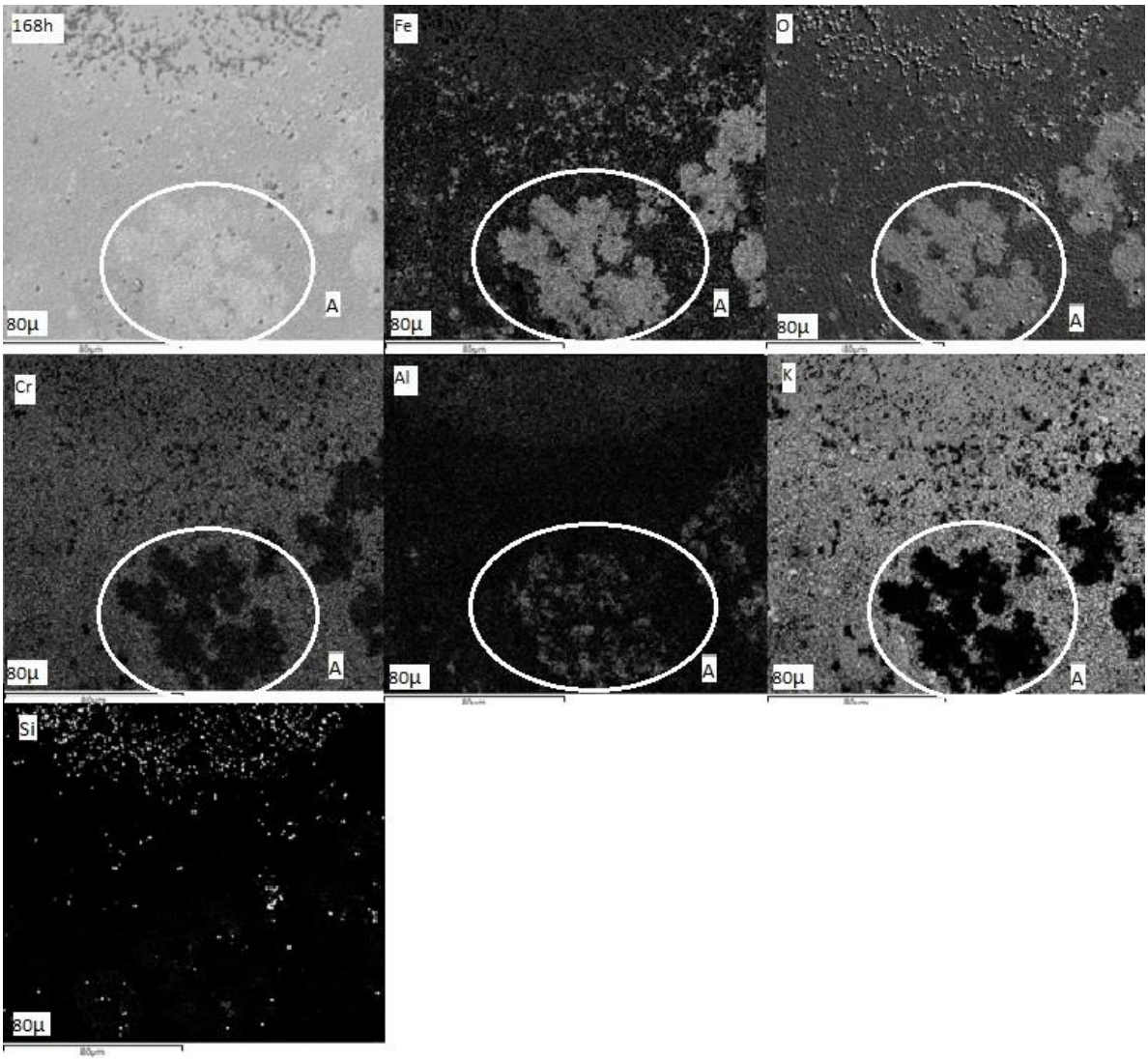

Figure 10: Energy Dispersive X-ray analysis mapping of APMT material applied with K_2CO_3 exposed for 168h at 600°C in O_2+H_2O.

5.6.2 Point analysis

Figure 18 show the surface of a FeCrAl-steel exposed for 1h. In addition, the regions where EDX analysis has been performed are marked. In Table 2, the compositions acquired from the different regions are shown. The EDX analyses comes from a depth of about 1 µm, thus if the oxide layer is thinner the composition will come both from the oxide layer and the bulk. Thus, to elucidate the composition of the oxide product on the surface, the contribution from the bulk needs to be adjusted for. All further observations are done with this in mind. Another thing to take into consideration is that C and O is difficult to analyze properly as the quantification of light elements is imprecise

Spectrum 1 & 2 which are the suspected K_2CO_3 formations only have significant amounts of K, O and C proving that this is in fact unreacted K_2CO_3. Spectrum 3 & 4 is the crater-like formations and show a slight decrease in Cr and K and a slightly higher amount of Fe when compared to spectrum 5 & 6 (the base oxide). The elemental composition proves that this surface is covered with a mixture of K_2CrO_4 and unreacted K_2CO_3 without any corroded iron present; all iron is from the bulk metal.

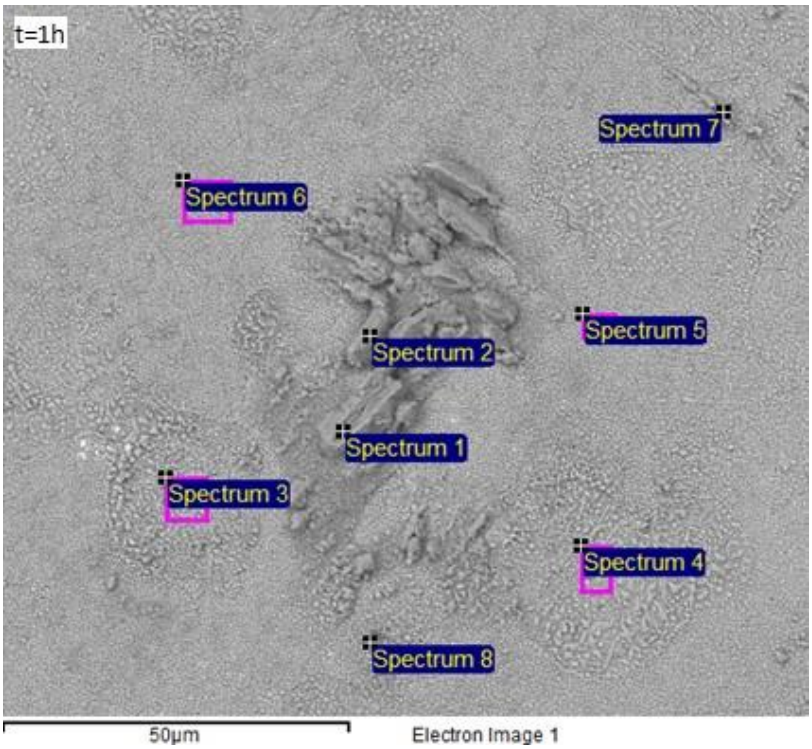

Figure 11: Energy Dispersive X-ray point analysis of APMT material applied with K_2CO_3 exposed for 1h at 600°C in O_2+H_2O.

Table 2: Energy Dispersive X-ray point analysis of APMT material applied with K_2CO_3 exposed for 1h at 600°C in O_2+H_2O.

Spectrum	In stats.	C %	O %	Al %	Si %	K %	Cr %	Fe %	Mo %
Spectrum 1	Yes	16	35	0	0	48	0	0	0
Spectrum 2	Yes	21	51	0	0	27	0	0	0
Spectrum 3	Yes	15	55	2	0	12	3	13	0
Spectrum 4	Yes	14	56	1	0	13	3	11	0
Spectrum 5	Yes	13	58	1	0	14	4	10	0
Spectrum 6	Yes	13	58	1	0	14	4	10	0

Figure 19 shows the surface of a sample exposed for 168h. Regions where EDX analysis has been conducted is marked and Table 3 contains the corresponding compositions. This is the same area that can be seen in Figure 17. Spectrum 3, 5 and 6 is the base oxide, K_2CrO_4. The lighter areas seen at the bottom of the picture is what was seen as darker areas ~~on~~ in Figure 17, and is here analyzed in Spectrum 1, 2 and 7. These areas, where the grains appear hollowed out, have a greater amount of Fe and lesser amount of Cr. Even when adjusted for the bulk metal the iron content is considerably higher, thus confirming the IC and XRD results of diminishing K_2CrO_4 in favor of Fe_2O_3. Spectrum 4 is an area rich in the silica rich dots mentioned in Figure 13.4 and have a high amount of Si.

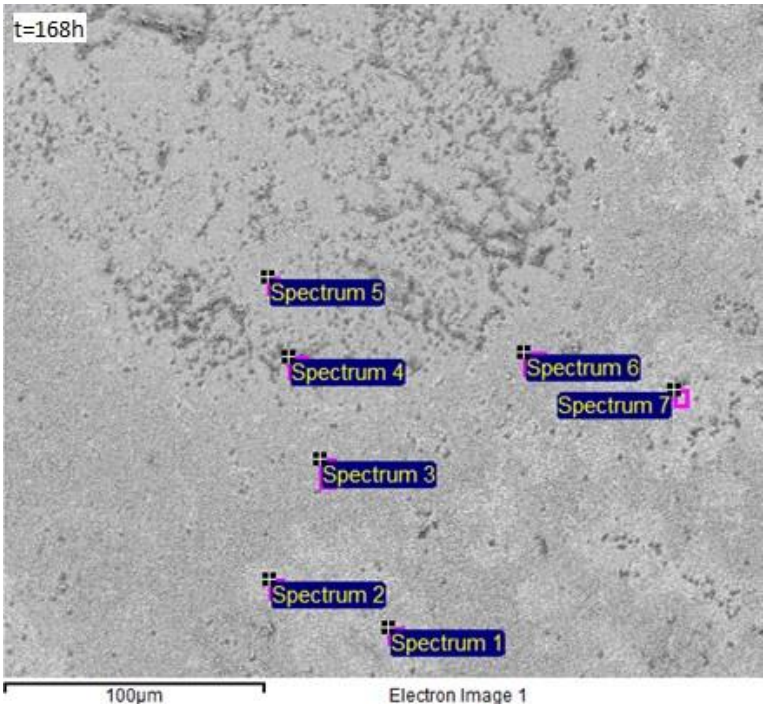

Figure 12: Energy Dispersive X-ray point analysis of APMT material applied with K_2CO_3 exposed for 168h at 600°C in O_2+H_2O.

Table 3: Energy Dispersive X-ray point analysis of APMT material applied with K_2CO_3 exposed for 168h at 600°C in O_2+H_2O.

Spectrum	In stats.	O %	Al %	Si %	K %	Cr %	Fe %	Mo %
Spectrum 1	Yes	65	1	4	1	3	26	0
Spectrum 2	Yes	65	2	5	2	3	23	0
Spectrum 3	Yes	64	0	2	13	8	12	1
Spectrum 4	Yes	65	1	7	12	8	8	0
Spectrum 5	Yes	64	1	1	15	7	12	1
Spectrum 6	Yes	64	1	2	16	9	9	1
Spectrum 7	Yes	65	2	4	1	4	24	0

6. Conclusion

6.1 Proposed mechanism of the breakaway corrosion in the presence of K_2CO_3

Figure 20 depicts the surface as it changes over time in hours.

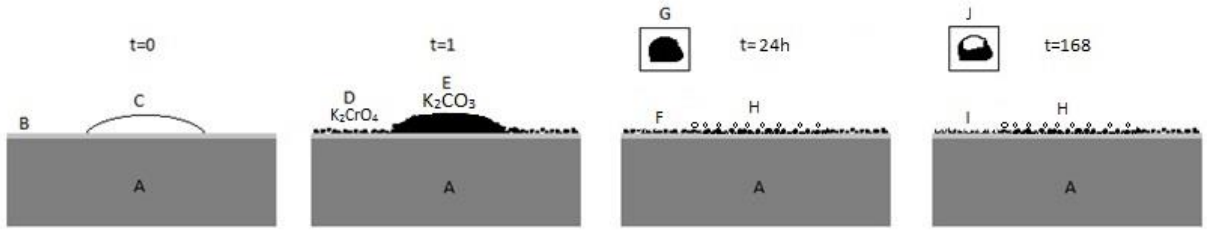

Figure 20: Schematic drawing of corroding FeCrAl exposed to K_2CO_2 from 0-168h.

At time zero, point A is the base material, whilst B is a thin film of iron-, chrome-, aluminum oxide ($(FeCrAl)O_3$). At C a large formation of K_2CO_3 can be seen, the dried remnants of a solution droplet.

After an hour of exposure (t=1h), all K_2CO_3 have diffused across the surface and corroded to form an uneven layer of small K_2CrO_4 grains, seen at D marked in black. These grains cover almost the entire surface excluding the areas where the K_2CO_3 formerly was present. At E we have large formations of unreacted K_2CO_3. The thin film below, $(FeCrAl)O_3$, is continually drained of chrome. The reaction for the K_2CrO_4 formation is as follows:

(2

$$½\ Cr_2O_3(s) + K_2CO_3(s) + 3\ ¼\ O_2 \rightarrow K_2CrO_4(s) + CO_2\ (g)$$

The interesting change that happened on the surface of the sample exposed for 24h is that there is no unreacted K_2CO_3 left. In their stead there are areas with white silica dots seen at H. Already in this picture tiny areas of iron oxide is visible at F.

The results from the IC and the XRD are not fully in agreement. The XRD peaks in K_2CrO_4 concentration after 72h whilst the IC peaks at 24h. This difference can be attributed to overlapping in the XRD diffractrogram spectra and that two different samples where used. The disappearance of K_2CrO_4 starts presumably between 72h and 168h. After a week, t=168, the most noticeable change is that a large portion of K_2CrO_4 grains is hollowed out across the entire surface. This is easier to see in the difference between individual grains illustrated in G and J. In certain areas the K_2CrO_4 oxide is completely depleted and pointy iron oxide (Fe_2O_3) is found to form at I.

The results are thus conclusive. The FeCrAl steel does not form a protective Al_2O_3 oxide layer and the steel seem to be vulnerable in K_2CO_3 rich environments. However, the silica rich formations seen in Figure 17 and 13.4 seem stable after 168h, even with a silica content as low as 1.3 at.%. An increased amount of silica may form a protective layer instead. This theory would need additional research to be confirmed.

7. Sources

i. Jones, D. (1996) *Principles and Prevention of Corrosion* Prentice-Hall, inc
ii. Kofstad, P. (1988) *High Temperature Corrosion*. Essex: Elsevier Applied Sience Publishers LTD.
iii. Birks N, Meier GH, Pettit FS. (2006) *Introduction to High-Temperature Oxidation of Metals*. Cambridge University Press
iv. Prescott R, Graham MJ. (1992) The Formation of Aluminum Oxide Scales on High-Temperature Alloys. *Oxidation of Metals*, vol. 38, nr. 3-4.
v. Jönsson B, Berglund R, Magnusson J, Hening P, Hättestrand M. (2004) High Temperature Properties of a New Powder Metallurgical FeCrAl Alloy. *Materials Science Forum*, vol. 461-464
vi. Jenkins R, Snyder RL. (1996) *Introduction to X-Ray Powder Diffractometry*. John Wiley Sons, inc.
vii. Goldstein JI, Newbury DE, Echlin P, Joy DC, Lyman CE, Lifshin E, Sawyer L, Michael JR (2003) *Scanning electron microscopy and X-ray microanalysis*. Springer.
viii. Fritz JS, Gjerde, DT. (2009) *Ion chromatography*. Wiley